NeuroImage: Clinical 9 (2015) 83–94

Contents lists available at ScienceDirect

NeuroImage: Clinical

journal homepage: www.elsevier.com/locate/ynicl

Mapping causal functional contributions derived from the clinical assessment of brain damage after stroke

Melissa Zavaglia[a,b,*], Nils D. Forkert[a,c], Bastian Cheng[d], Christian Gerloff[d], Götz Thomalla[d], Claus C. Hilgetag[a,e]

[a]Department of Computational Neuroscience, University Medical Center Eppendorf, Hamburg University, Martinistraße 52, Hamburg 20246, Germany
[b]School of Engineering and Science, Jacobs University Bremen, Campus Ring 1, Bremen 28759, Germany
[c]Department of Radiology, Hotchkiss Brain Institute, University of Calgary, 3330 Hospital Drive NW, Calgary, AB T2N 4N1, Canada
[d]Department of Neurology, University Medical Center Eppendorf, Hamburg University, Martinistraße 52, Hamburg 20246, Germany
[e]Department of Health Sciences, Boston University, 635 Commonwealth Ave., Boston, MA 02215, USA

ARTICLE INFO

Article history:
Received 7 April 2015
Received in revised form 3 July 2015
Accepted 15 July 2015
Available online 1 August 2015

Keywords:
NIHSS
Lesion inference
Multi-perturbation Shapley value Analysis (MSA)
Game-theory

ABSTRACT

Lesion analysis reveals causal contributions of brain regions to mental functions, aiding the understanding of normal brain function as well as rehabilitation of brain-damaged patients. We applied a novel lesion inference technique based on game theory, Multi-perturbation Shapley value Analysis (MSA), to a large clinical lesion dataset. We used MSA to analyze the lesion patterns of 148 acute stroke patients together with their neurological deficits, as assessed by the National Institutes of Health Stroke Scale (NIHSS). The results revealed regional functional contributions to essential behavioral and cognitive functions as reflected in the NIHSS, particularly by subcortical structures. There were also side specific differences of functional contributions between the right and left hemispheric brain regions which may reflect the dominance of the left hemispheric syndrome aphasia in the NIHSS. Comparison of MSA to established lesion inference methods demonstrated the feasibility of the approach for analyzing clinical data and indicated its capability for objectively inferring functional contributions from multiple injured, potentially interacting sites, at the cost of having to predict the outcome of unknown lesion configurations. The analysis of regional functional contributions to neurological symptoms measured by the NIHSS contributes to the interpretation of this widely used standardized stroke scale in clinical practice as well as clinical trials and provides a first approximation of a 'map of stroke'.

1. Introduction

Ischemic stroke is a common cause of brain injury that may lead to severe deficits in brain function, requiring substantial efforts in treatment and rehabilitation. Understanding the functional anatomy of acute stroke is an important prerequisite for clinical decision making, as well as for the guidance of stroke treatment in routine clinical practice and in the context of clinical trials (Saver et al., 1999). Moreover, the diverse behavioral and cognitive deficits resulting from strokes may be used for systematic inferences on the neural substrate of fundamental brain functions (De Freitas et al., 2009).

Today, a broad range of techniques exists to investigate the functions of the living brain through the correlation of behavior and cognition with brain activity, as revealed by functional imaging. However, inferences drawn from the behavioral impact of lesions remain a fundamental source of information about causal functional contributions of different brain territories; see Rorden and Karnath (2004) for a detailed review of traditional concepts as well as current approaches for lesion inference. Diverse statistical strategies for deriving lesion inferences by lesion behavior mapping have been described (Rorden et al., 2009), such as Voxel-based Lesion Symptom Mapping (VLSM) (Bates et al., 2003), Voxel-based analysis of lesions (VAL) (Rorden and Brett, 2000), or Multi-Variate Pattern Analysis (MVPA) (Smith et al., 2013).

Specifically, in VLSM and VAL, lesions are manually or automatically identified for each patient and used to derive patterns of damage through statistical map comparisons. The VLSM method, introduced by Bates et al. (2003), uses similar voxel-based procedures as employed in the analysis of functional neuroimaging data, by comparing patients with or without lesions in a given voxel with respect to differences in behavioral measures, yielding a t-statistic for each voxel. The method can be modified

Abbreviations: CT, computer tomography; DWI, diffusion weighted imaging; MCA, middle cerebral artery; MRI, magnetic resonance imaging; MAPP, Multi-Area Pattern Prediction; MSA, Multi-perturbation Shapley value Analysis; MVPA, Multi-Variate Pattern Analysis; NIHSS, National Institutes of Health Stroke Scale; SVM, support vector machine; VAL, voxel-based analysis of lesions; VLSC, VOI-based Lesion Symptom Correlation; VLSM, Volume-based Lesion Symptom Mapping; VBM, voxel-based morphometry; VOI, volume of interest.

* Corresponding author at: Department of Computational Neuroscience, University Medical Center Eppendorf, Hamburg University, Martinistraße 52, Hamburg 20246, Germany. Tel.: +49 40 7410 52938; fax: +49 40 7410 54882.
E-mail addresses: m.zavaglia@uke.de (M. Zavaglia), n.forkert@uke.de (N.D. Forkert), b.cheng@uke.de (B. Cheng), gerloff@uke.de (C. Gerloff), thomalla@uke.de (G. Thomalla), c.hilgetag@uke.de (C.C. Hilgetag).

http://dx.doi.org/10.1016/j.nicl.2015.07.009

into a Voxel-based Lesion Symptom Correlation (VLSC) approach, by relating lesion patterns to behavioral measures through correlations, rather than through statistical group comparisons. VAL is also similar to VLSM, but compares lesion locations between a group of patients with behavioral deficit and a group of patients with brain damage, but without deficit. Finally, Smith et al. (2013) introduced an inference approach based on machine learning, called Multi-Variate Pattern Analysis (MVPA), to predict the presence or absence of spatial neglect based on brain injury maps using linear and nonlinear support vector machines (SVMs).

As a further alternative, an inference approach based on game theory has been proposed for the analysis of behavioral effects resulting from multi-lesion patterns. This approach, Multi-perturbation Shapley value Analysis (MSA) (Keinan et al., 2004a) is a rigorous mathematical method to assess functional localization from perturbation data. It defines and calculates the contributions of network elements, specifically brain regions, from a dataset of multiple lesions (or perturbation experiments) and their associated performance scores. The regions are considered as 'players' in a game who interact to achieve a behavioral outcome. The approach can also be used to quantify the interactions of the network elements. The MSA approach has found a wide range of applications in neuroscience, such as the analysis of reversible deactivation experiments (Keinan et al., 2004b) and computational models of neurocontrollers (Keinan et al., 2006), as well as applications in biochemistry and genetics, for instance, the localization of function in gene-regulatory networks from gene knockouts (Kaufman et al., 2005). In a proof-of-concept study for clinical applications, Kaufman et al. (2009) applied MSA to lesion data and line bisection test scores of 23 right-hemisphere stroke patients.

Lesion inference methods have been frequently applied to study specific neurological symptoms, such as neglect (Smith et al., 2013; Karnath et al., 2001) or aphasia (Kümmerer et al., 2013). However, there is still only a limited understanding of the clinical consequences of acute stroke lesions in specific brain regions with respect to the whole picture of neurological symptoms. Moreover, while standardized clinical rating scales, such as the National Institutes of Health Stroke Scale (NIHSS, Brott et al., 1989), are widely used to characterize the functional abilities of patients and guide treatment decisions, only little is known about how scores in these scales relate to the involvement of specific brain lesions in acute brain ischemia (Menezes et al., 2007).

In the present study, we applied MSA systematically to a large and representative sample of patients with acute stroke, to derive contributions of bilateral cortical and subcortical regions to a broad range of neurological symptoms as captured by the NIHSS, which quantifies basic behavioral and cognitive capabilities through a test battery of simple sensory, motor, language, and attention tasks. We also compared the regional functional contributions indicated by MSA with those computed by other methods that relate stroke lesion patterns to behavior, such as VLSM, VLSC (Saver et al., 1999) and multi-variate pattern prediction. Our principal goals in this study were, first, to understand the functional contributions of different brain regions to the broad spectrum of neurological symptoms as reflected by the NIHSS, representing the most widely used standardized stroke symptom rating scale. Second, we wanted to assess the suitability of the MSA approach for processing clinical lesion data and use MSA to study the functional contribution of large-scale brain regions to basic behavioral functions, based on functional deficits after lesion damage. Third, our study compared the inferences provided by MSA with those of alternative approaches and investigate potential biases in the inferences due to a restricted sample of available lesion configurations.

2. Methods and data

2.1. Behavioral and lesion image data

In the present study, we used a large multi-center set of stroke patient data to investigate functional contributions of eight bilateral volumes of interest (VOIs), defined by the MNI structural atlas (Collins et al., 1995): caudate (CAU), insula (IN), frontal (FR), occipital (OCC), parietal (PAR) and temporal lobes (TEM), as well as putamen (PUT) and thalamus (TH). The MRI and clinical data used in this study (N = 148) constitute a subset of the patient data included in the *PRE-FLAIR* study, which is a multi-center observational study designed to analyze the combined use of FLAIR (fluid attenuated inversion recovery MR imaging) and DWI (diffusion-weighted MR imaging) for identifying patients with acute ischemic stroke within 4.5 h of symptom onset (Thomalla et al., 2011). All patients in this study were studied within 12 h of witnessed stroke onset, and severity of neurological deficit on admission was assessed using the global NIHSS. The DWI sequences, which were used as the basis for lesion segmentation, were acquired by applying diffusion gradients in three directions with strong diffusion weighting (b-value = 1000 s/mm^2). Detailed information about the imaging parameters can be found in Thomalla et al. (2011).

The NIHSS is a rating scale resulting from a standardized neurological examination quantifying symptom severity in acute stroke (Brott et al., 1989). The NIHSS comprises 11 items scoring specific abilities with values ranging between 0 (no symptoms, correct performance of task) and 2–4 (maximum symptom severity for corresponding item): Level of Consciousness, Horizontal Eye Movement, Visual field, Facial Palsy, Motor Arm, Motor Leg, Limb Ataxia, Sensory, Language (Aphasia), Dysarthria, Extinction and Inattention. Higher scores indicate more severe impairment. A sum score is calculated from the individual score values and ranges from 0 to 42. The NIHSS is widely used for standardized clinical assessment of stroke patients in routine clinical practice as well as in stroke research and is also frequently used to include or exclude patients in acute stroke trials.

2.2. Lesion image processing

For the purpose of a quantitative lesion analysis, the infarct lesions were semi-automatically segmented by an experienced neurologist (B.C.) for each DWI image sequence acquired with strong diffusion weighting in a standardized fashion (Cheng et al., 2013). More precisely, the visible lesions were manually surrounded in each axial slice including a safety margin by interactively placing points at the border of the visible stroke lesion. These points were automatically connected using a cubic spline interpolation and points were manually adjusted if required. After contour definition in each affected slice, a binary volume was generated using all spline-based contours. A second healthy volume of interest was then placed in the contralateral unaffected hemisphere in the corresponding brain tissue in the same manner. The resulting healthy volume of interest was defined in a way that it represents an approximation of the mirrored lesion volume. This healthy volume of interest was then employed for calculating the corresponding mean μ and standard deviation σ of the DWI signal intensities. These values were used for refining the defined coarse DWI lesion volume of interest by rejecting voxels with a DWI signal intensity $< \mu + 2\sigma$, such that only the actual lesion was covered by the resulting segmentation.

Due to different positions of the acute stroke patients within the MR scanner, different inter-subject head anatomies and variations regarding the spatial resolution of the DWI image sequences, a registration of the datasets into a reference space was necessary to quantify the number of lesioned voxels in different brain regions of interest that are defined in the reference space. Therefore, the 1 mm^3 MNI ICBM152 brain atlas, which has been designated as the standard template by the International Consortium for Brain Mapping, was used for definition of the reference space (Collins et al., 1995). To overcome the problem of differences regarding the signal intensities and visible tissues in the MNI brain atlas, which was constructed based on T1-weighted image sequences from 148 healthy subjects, and in the T2-weighted DWI image sequences, an iterative closest point (ICP) registration approach (Besl and McKay, 1992) was used in this work, which is illustrated in Fig. 1. Particularly, an

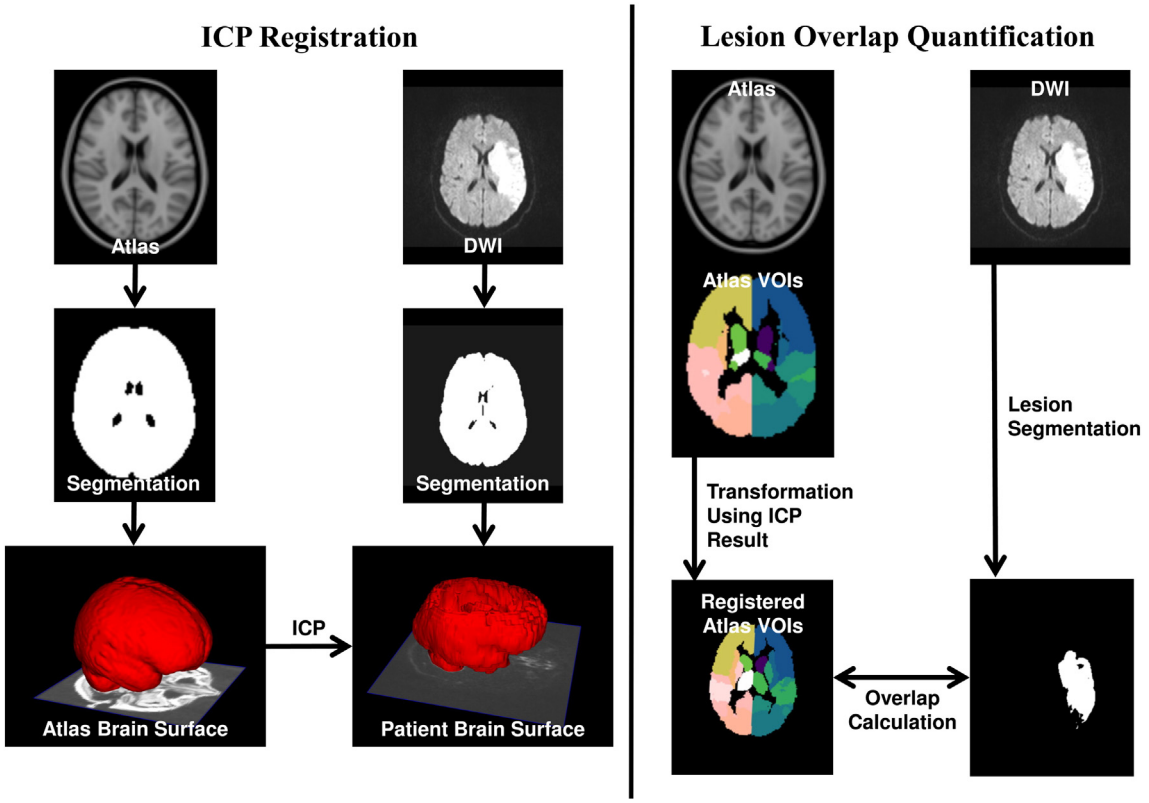

Fig. 1. Pipeline for registration and quantitative lesion image processing. Left: the brain tissue is automatically segmented in the DWI dataset and used to generate a 3D surface model. A corresponding 3D surface model is also generated based on the atlas brain segmentation, which is then used to calculate the optimal transformation to the DWI dataset using an iterative closest point algorithm (ICP). Right: the resulting transformation is employed to align the structural regions defined in the atlas with the patient-specific DWI dataset. After semi-automatic segmentation of the lesion in the DWI dataset, the transformed structural brain regions can be used to calculate the individual lesion overlap values. The lesion overlap visualization also depicts the eight bilateral VOIs used in the present study.

adapted version of the brain segmentation method described in Forkert et al. (2009) was used to extract the brain tissue from each DWI dataset with strong diffusion weighting of the acute stroke patients. The resulting brain segmentations were employed for generation of the corresponding 3D surface models using the Marching Cubes algorithm (Lorensen and Cline, 1987). The Marching Cubes algorithm was also used for generation of a surface model from the brain segmentation of the MNI brain atlas. After this step, the brain surface model of the MNI brain atlas was registered to each patient brain surface model employing the ICP algorithm using an affine transformation. After surface-based ICP registration, the resulting affine transformation was used to adapt the brain regions defined in the MNI brain atlas to each patient.

Finally, the overlap (in %) between the transformed 16 anatomical structural regions as defined in the MNI structural atlas (Fig. 1) and the patient-specific acute ischemic stroke lesion was calculated for each patient. The choice of the volumes of interest was motivated by the need of the subsequent MSA approach for a moderate number of included regions, the ready availability of such a coarse parcellation in the MNI atlas, as well as the requirement of an exhaustive parcellation of the whole brain in order to exclude hidden functional contributions. The resulting dataset was composed of 148 patient cases with different patterns of lesioned VOIs (76 patients left-only, 71 patients right-only) and the corresponding global NIHSS values of the patients. One further case without lesions in any of the VOIs and a NIHSS of zero was included in both the left and right hemispheric group, serving as a baseline value for the NIHSS in healthy controls. As there were no cases with lesion overlap between the hemispheres, left- and right-hemispheric lesion cases were analyzed separately.

2.3. Original versus complete-predicted dataset

The original-graded dataset described in Section 2.2 is composed of 76 left-hemisphere-only and 71 right-hemisphere-only lesion patients, as well as one further patient without an apparent lesion, which was included in the left as well as in the right hemispheric set, resulting in 77 and 72 patients, respectively. For each patient, the NIHSS score (ranging from 0 to 21, where 0 indicates the absence of behavioral deficits and 21 indicates the most severe impairment found) as well as the graded lesion overlap measure for each of the eight VOIs in the affected hemisphere were available. Thus, the dataset comprised graded values of lesions for each VOI together with the corresponding NIHSS and, as is typical for clinical datasets, did not represent the full set of all possible combination of binary lesions of the VOIs (where each VOI can be lesioned, "0", or intact, "1") but presents an opportunistic sample (*original-sample dataset*). In order to balance the occurrence of different lesion configurations, we expanded the sample to the full set of all possible $2^N = 256$ binary lesion configuration cases (where $N = 8$ is the number of VOIs for each hemisphere and each VOI can be lesioned or intact). Then, we used a machine learning predictor in order to obtain the behavioral scores corresponding to the full set of all possible binary configurations (*complete-predicted dataset*). Since the scores are graded from 0 to 21 (i.e., 22 possible classes) we used a multi-class predictor; specifically a linear kernel support vector machine (SVM) for multi-class classification, implemented in LIBSVM (Chang and Lin, 2011), trained on the available graded original-sample dataset after binarization (*binary-sample dataset*). As a pragmatic approach, the binary-sample dataset used for training the predictor was obtained from the original-graded dataset for each hemisphere separately, by defining each VOI as lesioned ("0") or intact ("1") depending on whether relative

lesion size was larger or smaller than the median value of all non-zero percentages of lesioned voxels for that VOI. In order to assess the statistical power of the multi-class predictor, we performed a leave-one-out cross-validation by iteratively using each single case from the training data as the validation data and all the remaining cases as the training data. Specifically, we performed the leave-one-out cross-validation on both left (77 cases) and right (72 cases) training sets by computing the RMSE (Root Mean Square Error) and the accuracy (obtained with a maximum tolerance error between real and predicted score of ± 3). For the left hemisphere the RMSE and accuracy were, respectively, 5.6 and 54%, and for right hemisphere 6.0 and 53%. These classification accuracies are considerably higher than the statistical chance levels, which were determined by calculating the precise chance level (NIHSS $\pm$ 0) for each NIHSS value, by dividing each NIHSS value frequency by the total number of patients and subsequent addition of the chance levels ± 3 for each NIHSS score. According to this procedure, a mean chance level of 30.22% for the left hemisphere (ranging from 12.98% to 54.54%) and 30.49% for the right hemisphere (ranging from 4.17% to 45.83%) was found for this patient cohort.

We then used the leave-one-out technique to estimate the variability of the prediction, by iteratively excluding each individual left- or right-hemispheric case from the prediction of the behavioral scores for the complete-predicted dataset, resulting in 77 separate predictions for the left and 72 predictions for the right hemisphere.

2.4. Multi-perturbation Shapely value Analysis (MSA)

The MSA approach is a rigorous method for assessing causal function localization from multiple perturbation data, based on coalitional game theory (Shapley, 1953). In general, the system elements (here, VOIs) can be seen as players in a game, and a *perturbation configuration* represents a subset of elements that are perturbed concomitantly. The *coalition* of players is represented by the group of elements that are left intact. For each configuration, the performance of the system, which can be seen as the *worth* of the coalition, is measured. Since NIHSS represents the severity of neurological deficit and MSA requires a score reflecting behavioral ability, we used the inverse of NIHSS (maximum NIHSS score minus current NIHSS score) as an indicator of functional performance. The aim of the analysis is to assign values that represent the elements' contribution to, or importance for, the overall function. The contribution value of a player, formalized as the Shapley value (Shapley, 1953), represents the difference between the worth of coalitions which contain the element and the worth of coalitions which do not contain it.

More formally, in a system composed of $N=\{1,\ldots\ldots,n\}$ elements performing a task, it is possible to define a coalition S, where $S \subseteq N$, and a *performance score v(S)*, which is a real number representing the performance measured for the perturbation configuration in which all the elements in S are intact and the rest perturbed. The definite value in game theory and economics for this type of coalitional game is the Shapley value (Shapley, 1953). The *marginal importance* of player i to a coalition S, with $i \notin S$, is represented as $\Delta_i(S) = v(S \cup \{i\}) - v(S)$. The Shapley value of each player $i \in N$ is defined by Eq. (1), where $\Re$ is the set of all $n!$ orderings of N and $S_i(R)$ is the set of players preceding i in the ordering R.

$$\gamma_i(N, v) = 1/n! \sum_{R \in \Re} \Delta_i(S_i(R)) \tag{1}$$

If we consider that all the players are arranged in some order (all orders being equally likely), the Shapley value can be seen as the marginal importance of a player i to the set of players that precede it. Here, a configuration is a binary vector of length n, with $c_i = 1$ if $i \in S$ or $c_i = 0$ if $i \notin S$, i.e., an indicator vector for the unperturbed elements. For a more detailed description of the MSA see Keinan et al. (2004a).

When all possible 2^N perturbation configurations are known, the Shapley value can be computed using Eq. (1), or as a summation over all 2^N configurations, weighted by the number of possible ordering of the elements (*Full Information MSA*). If the full set of all binary lesion configurations cases with corresponding performance scores (256 configurations in the present study) is not known, it can be obtained with the help of a predictive algorithm as described in Section 2.3, resulting in a complete-predicted dataset and *Predicted MSA* values. By applying the leave-one-out approach, we computed the average MSA contributions across 77 predictions of the complete 256 behavioral scores for the left hemisphere and 72 predictions for the right hemisphere.

2.5. Regional interactions: redundancies and synergies

Lesion inferences, in addition to identifying the contributions of individual elements, may also be used to investigate interactions among elements. In particular, such interactions can reveal functional redundancies between regions that indicate functional overlap, as well as synergistic relations. In order to describe the two-dimensional functional interactions between elements within the framework of MSA, we need to define the following quantities. The Shapley value of element i in the subgame of all elements without j is given by $\gamma_{i,\bar{j}}(N, v)$. Intuitively, it represents the average marginal importance of element i when element j is lesioned. In the same way, we can define the Shapley value of element j in the subgame of all elements without i by $\gamma_{j,\bar{i}}(N, v)$. If we jointly consider the two elements i and j, as if they form a unique, joined element, it is possible to define the average marginal importance of this element with $\gamma_{(i,j)}$. Then, the two-dimensional interaction between elements i and j can be defined as

$$I_{i,j} = \gamma_{(i,j)} - \gamma_{i,\bar{j}} - \gamma_{j,\bar{i}} \tag{2}$$

which quantifies how much the average marginal importance of the two joined elements is larger or smaller than the sum of the average marginal importance of each of them when the other one is perturbed. This is a symmetric definition, $I_{i,j} = I_{j,i}$. Thus, the interaction value indicates how much the whole (i.e., the contribution of the joined pair of regions) is greater than the sum of the parts (i.e., the sum of the individual functional contributions). When the interaction is negative, there exists a redundancy or (partial) functional overlap between the two elements. By contrast, when the interaction is positive, the two elements jointly perform better than individually, which indicates a synergistic interaction. These relations also provide an indication on the choice of regions of interest in the lesion analysis, because regions with redundant interactions could be merged or reshaped, while synergistically interacting regions should be kept separate. See Keinan et al. (2004a) for further details.

2.6. Comparison approaches of lesion inference

Initially, we visualized the distribution of stroke lesions using two different approaches. The first one was *Lesion Overlap*, which is a widely used, straightforward assessment of lesion patterns, e.g. Karnath et al. (2001), based here on the MNI atlas. Specifically, it shows the overlap (in %) between the voxels defined in the MNI ICBM152 structural atlas space and the patient-specific acute ischemic stroke lesion. The second approach, *Median VOI Lesion Overlap*, is identical to Lesion Overlap, but is based on VOIs, rather than voxels. It shows the normalized overlap of lesions within the parcellation of the 2×8 VOIs in MNI ICBM152 standard atlas space. The two overlay measures allow a straightforward assessment of relative lesion size and frequency (Fig. 2). However, it needs to be pointed out that lesion overlays are insufficient for drawing reliable inferences from lesion data (Rorden and Karnath, 2004). Therefore, we only used them for an initial visualization of the lesion patterns and

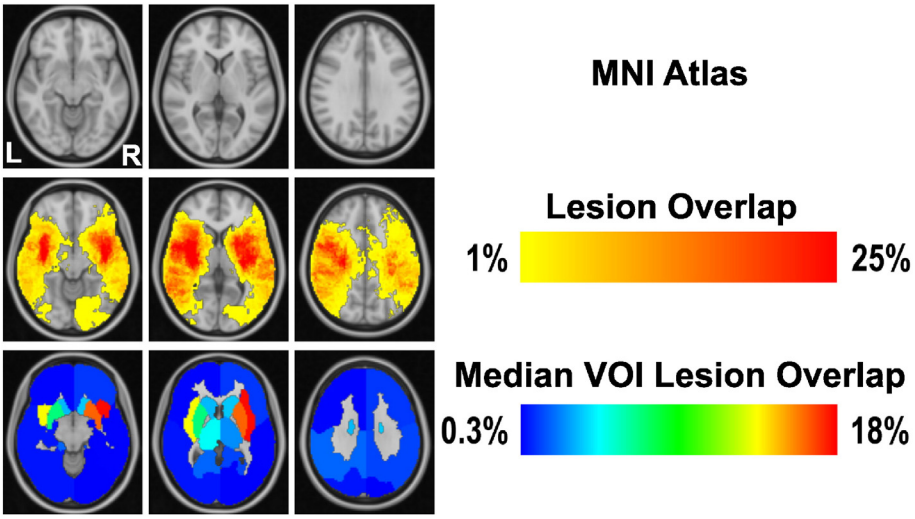

Fig. 2. Lesion Overlap in MNI152 standard atlas space. From top to bottom, representation of MNI atlas (we selected three representative slices from the MNI atlas that covered all structural regions), Lesion Overlap and Median VOI Lesion Overlap, in neurological convention. While the lesion overlap focuses at the scale of voxels, median VOI lesion overlap shows the relative (median percentage) infarction within the confines of the predefined 2 × 8 VOIs.

performed detailed comparisons of the MSA outcomes using more principled approaches.

In particular, we compared the functional contributions indicated by MSA with those shown by three alternative methods of lesion inference. It is worth noting that, in contrast to MSA, these three methods do not require the complete-predicted dataset, but can also be applied to the sample datasets (original or binary). The first approach, Voxel-based Lesion Symptom Mapping (VLSM) (Bates et al., 2003) was originally introduced at voxel level. Presently, it was applied to VOIs, preserving the acronym VLSM for *Volume-based Lesion Symptom Mapping*. The VLSM approach makes use of binary information about the intactness or lesion of each VOI. The binary-sample dataset was obtained by using a median threshold for each VOI, as explained in Section 2.3. We separately analyzed left- and right-brain-damaged patients and performed a VLSM analysis by computing a t-score for each VOI, assessing differences in the performance scores of patients in which a particular VOI was either lesioned or intact. As *performance score v* of each case *i*, we considered the inverse of the global NIHSS ($v_i = max(NIHSS) - NIHSS_i$). Subsequently, we applied VLSM also to the complete-predicted dataset described in Section 2.3.

The second comparison method was the approach of *VOI-based Lesion Symptom Correlation* (VLSC). The correlation between relative (or absolute) lesion size and global NIHSS is a straightforward metric that provides helpful preliminary information about the relationship between lesions of individual regions and behavior, similar to VLSM. However, while VSLM makes use of binarized data, the VLSC is computed from the original-graded dataset, considering only the non-zero lesion cases (i.e., cases in which the VOIs have any damage) and corresponding NIHSS. We used Spearman rank correlations, in line with the ordinal nature of the present data. To explore the potential influence of the factor of total lesion volume on these correlations, we also performed partial correlations for all VOIs using total lesion size as a control.

The third method was the newly devised *Multi-Area Pattern Prediction* (MAPP) approach which represents one possible way to compare MSA and MVPA (Smith et al., 2013) outcomes. While not identical to MVPA, this analysis is performed in the same spirit. MAPP operates by computing the leave-one-out cross-validation for each hemisphere, as described in Section 2.3, but with eight different datasets, obtained respectively by removing each single VOI one at a time. As for the VLSM, MAPP makes use of the binary-sample dataset and the corresponding performance scores. Specifically, the RMSE is computed for eight different datasets composed each of 77 cases for the left hemisphere and 72 cases for the right hemisphere (as described in Section 2.3), but each comprising seven VOIs instead of eight. In this way, it is possible to obtain a measure of how "important" each VOI is for the prediction procedure (i.e., by its individual contribution to the prediction error). Specifically, we computed a $\Delta_{prediction\_error}$ for each VOI, as the difference between the RMSE computed without the single VOI and the RMSE computed with the complete set of all VOIs.

3. Results

3.1. Data overview

In Table 1 we present clinical and imaging data for all patients included in the study (N = 148 patients).

The VOIs used in the study are indicated in Fig. 1. Fig. 2 shows the MNI atlas and the outcomes of the Lesion Overlap and Median VOI Lesion Overlap approaches, using neurological convention. The lesion overlays (relative across all cases) indicated that maximally 25% of all patients had a lesion in a given voxel and that all VOIs were damaged, to different extent. The measures also indicated that, on a relative scale, the subcortical regions were most frequently affected, especially in the right hemisphere. This hemispheric difference was even more pronounced in the VOI-based overlap.

Fig. 3 shows the absolute and relative lesion sizes of the 2 × 8 VOIs in all 148 patients together with the associated behavioral scores (global NIHSS). The absolute lesion size, in panel (a), was graded from zero to a value of 13,202, which represents the maximum number of lesioned voxels of a VOI in the dataset, while the relative lesion size of VOIs, in panel (b), was graded from 0 to 100%. The NIHSS ranged from zero to 21, where 0 indicates the absence of behavioral deficits and 21 indicates the most severe impairment found in the patient sample, out of a possible maximum score of 42.

Table 1
Clinical and imaging data of the present study.

	N	Mean	Minimum	Maximum	95% CI	Standard deviation
Female gender	70 (47%)					
NIHSS	148	8.9	0	21	8–9.8	5.62
Time to MRI [min]	148	269	10	720	237–300	194.64
Age at onset [y]	148	64.1	23	98	61.7–66.7	15.18
DWI lesion volume [ml]	148	19.4	0	179	14.7–24.1	29.93

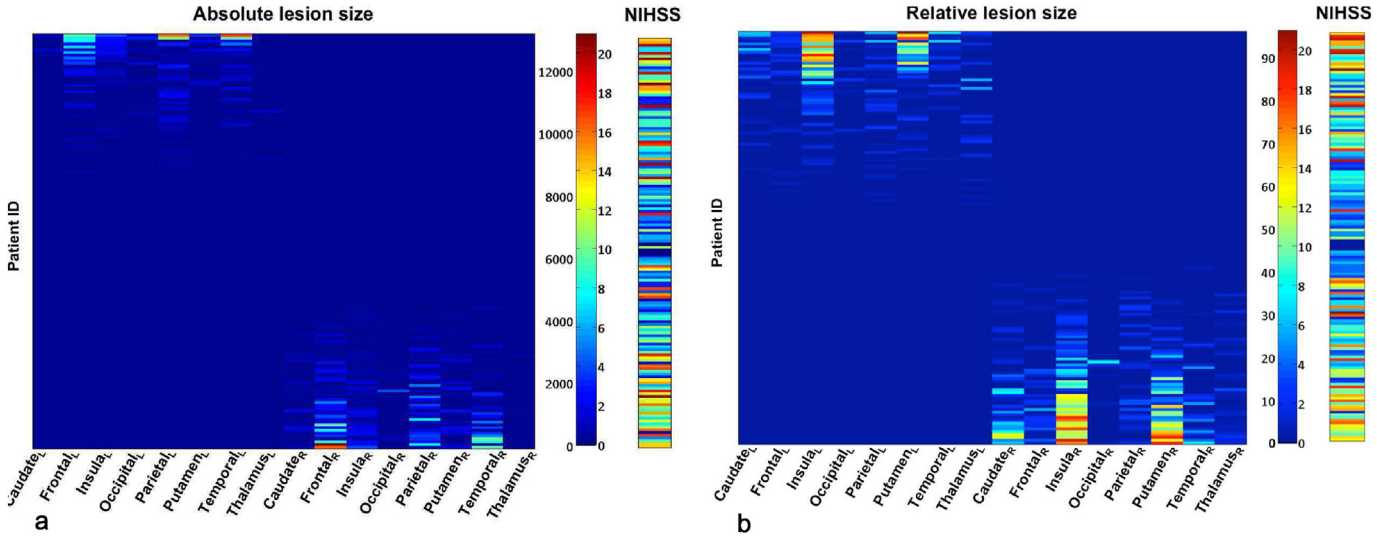

Fig. 3. Lesion size of VOIs and associated NIHSS. (a) Absolute and (b) relative lesion size (in % of lesioned voxels) of 2 × 8 VOIs and associated global NIHSS values for 148 patients. In each panel, the color scale indicates on its left axis the absolute (graded from zero to 13,202) or relative (graded from 0 to 100%) lesion size and on the right axis the range of associated NIHSS values (from zero to 21). The 148 cases (indicated by patient ID) were separated into left- and right-hemispheric lesions by sorting in descending order the difference between total lesion size in the left and right hemispheres.

Apparent are the clear segregation into left- and right-hemispheric lesions and the general correlation of lesion size with NIHSS, with higher scores being associated with larger lesions.

As a baseline for the subsequent lesion correlation analysis, we computed the Spearman rank correlation between global NIHSS and total lesion size, calculated separately for the 77 left and 72 right hemisphere lesion cases, as the sum of relative or absolute values of lesioned voxels over all VOIs. The rank correlation between total absolute lesion size and NIHSS was 0.42 ($p = 1.32 \times 10^{-4}$) and 0.42 ($p = 2.52 \times 10^{-4}$) for the left and right hemisphere, respectively. The correlation between total relative lesion size and NIHSS was 0.54 ($p = 3.74 \times 10^{-7}$) and 0.46 ($p = 4.54 \times 10^{-5}$) for the left and right hemisphere, respectively.

3.2. MSA functional contributions

Fig. 4 shows the normalized mean MSA contribution values for the inverse global NIHSS. As left- and right-hemispheric lesions were strictly separated in the present patient sample, contributions of VOIs were computed separately for the left and right hemisphere. Standard deviation bars were derived from the leave-one-out technique during the prediction of performance scores (cf. Section 2.4). Positive contributions indicate that VOIs contribute to the success of the performance of a task. Thus, if they are lesioned, the performance is lowered. By contrast, negative contribution values imply that regions may be hindering the performance of a task.

MSA indicated that all contributions (except for the right temporal lobe) were significantly different from zero, performing a t-test against the alternative of zero mean (after Bonferroni correction, adjusted $p < 0.0063$). Subcortical regions, such as the bilateral caudate and left insula, together with the bilateral parietal and frontal lobes, were inferred to make the strongest contributions to brain functions as reflected in the NIHSS, while negative contributions were seen for the right putamen and left thalamus. In other words, lesions in the caudate, insula, parietal or frontal lobes contributed most strongly to the neurological symptoms as assessed by the NIHSS, while lesions in the right putamen and left thalamus were contributing less to the behavioral score.

3.3. Regional interactions

Based on the MSA values, functional interactions were computed from the lesion data. Fig. 5 shows the mean functional interactions based on the contribution values for the global inverse NIHSS pictured in Fig. 4. The quantities are mean values, computed from the contributions values obtained with the leave-one-out technique. For the left hemisphere, the strongest positive interactions that are significantly

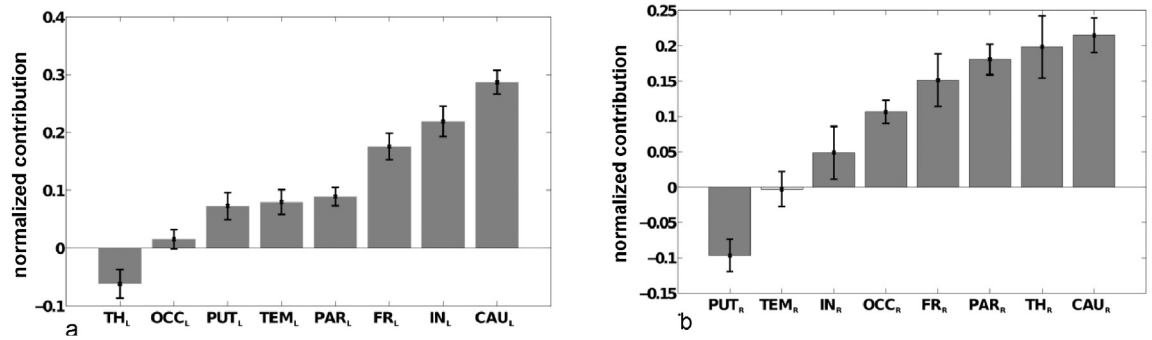

Fig. 4. Relative functional contributions indicated by MSA. Normalized mean MSA contribution values (±SD) for inverse global NIHSS, computed separately for left- and right-sided lesion cases, using the binary dataset for the prediction of all performance scores corresponding to the full lesion configuration set by linear kernel SVM. Significant contributions (after Bonferroni correction) are shown in gray (all contributions are significant except for right temporal lobe).

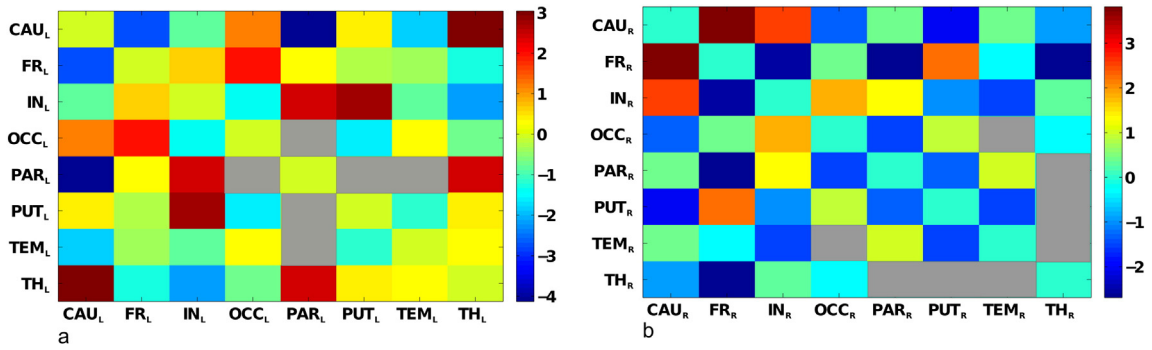

Fig. 5. Functional interactions among VOIs. Matrix representation of (symmetric) mean functional interactions of (a) left and (b) right VOIs. The color scales indicate the range of variation of left (a) and right (b) mean functional interactions. In (a), all interactions are significantly different from zero (after Bonferroni correction), except between parietal–occipital, parietal–putamen and parietal–temporal regions (represented as gray entries in the matrix). In (b), all interactions are significantly different from zero (after Bonferroni correction), except between temporal–occipital, temporal–thalamus, thalamus–parietal, thalamus–putamen regions (represented as gray entries in the matrix).

different from zero (after Bonferroni correction, adjusted $p < 0.0018$) were between the insula and putamen, insula and parietal cortex, thalamus and caudate, thalamus and parietal cortex, as well as the frontal and occipital cortex. The strongest negative interactions, indicating functional redundancies, were found between the parietal cortex and caudate, as well as the frontal cortex and caudate. For the right hemisphere, the strongest positive interactions significantly different from zero (after Bonferroni correction, adjusted $p < 0.0018$) were found between the caudate and frontal cortex, caudate and insula, and frontal cortex and putamen. The strongest negative interactions were found between the frontal cortex and insula, thalamus and parietal cortex, respectively.

3.4. Comparison approaches of lesion inference

Fig. 6 shows the outcomes of the Multi-perturbation Shapley value Analysis (same quantities as depicted in Fig. 4), Volume-based Lesion Symptom Mapping and VOI-based Lesion Symptom Correlation, applied separately to the left- and right-hemispheric datasets and shown in the reference space of the MNI atlas, using neurological convention. Black stripes indicate VOIs without a significant value.

VLSM was applied to the binary-sample dataset, and the resulting t-score is represented for each VOI. It is interesting to note that after Bonferroni correction (adjusted $p < 0.0063$), lesions of right VOIs appear to have no significant effect on the performance score (indicated by overlapping black grid), while lesions of the caudate, insula, putamen and frontal lobe in the left hemisphere have a highly significant relation with behavior.

The VLSC, represented by the Spearman rank correlation coefficient between relative lesion size (excluding zero lesions) and global NIHSS for each VOI, is represented in the bottom row. Correlations that were significantly different from zero ($p < 0.05$) existed with relative lesions of the bilateral caudate, left insula, left putamen, and right frontal lobe. Interestingly, the left VOIs showed higher correlations than the right ones. Moreover, correlations of absolute lesion size of the left insula ($\rho = 0.42$, $p = 0.0022$), left caudate ($\rho = 0.50$, $p = 0.0018$) and left putamen ($\rho = 0.50$, $p = 0.0008$) with NIHSS were higher than the baseline correlation of the total absolute left lesion size with NIHSS ($\rho = 0.42$, $p = 1.32 \times 10^{-4}$; Section 3.1). As indicated by the color scale, the correlation coefficients showed a similar pattern as the VLSM t-scores.

The baseline correlations of total (absolute and relative) lesion size with NIHSS (Section 3.1) indicated that total lesion volume may be an important confound in the analysis. In order to take this factor into account, we performed control calculations using partial correlations for all VOIs instead of bivariate correlations, with total absolute lesion size as a control factor. These calculations (shown in the Supplementary Material) indeed reduced the partial correlations as compared to the bivariate correlations when taking into account total lesion size. Moreover, the previously significant bivariate correlation of right frontal cortex with NIHSS was no longer significant. Generally, however, the

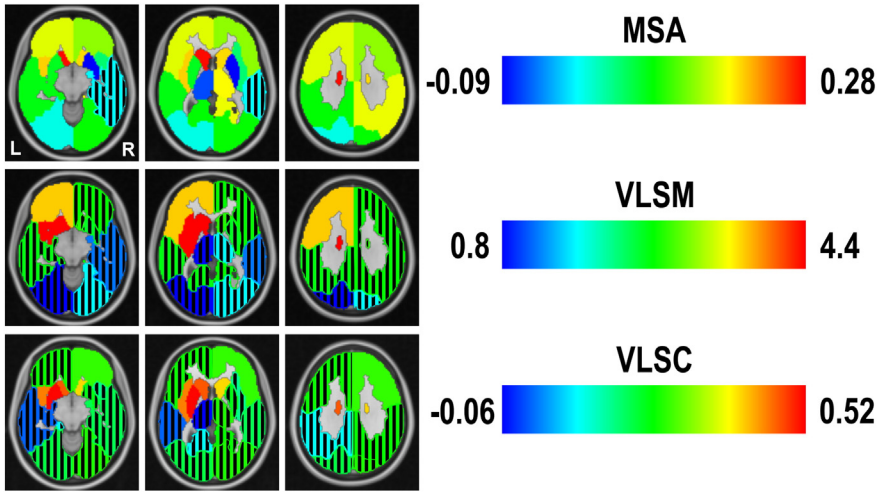

Fig. 6. Comparison approaches of lesion inference. Comparison based on the MNI atlas (we selected 3 slices from the MNI atlas that are representative to cover all structural regions) between correlation coefficients computed with VOI-based Lesion Symptom Correlation, t-scores obtained with Volume-based Lesion Symptom Mapping and normalized mean contribution values for global inverse NIHSS obtained with MSA. The color map is the same for all measures, but at different scales. Black stripes indicate VOIs without a significant value.

patterns of bivariate and partial correlations were very similar (Supplementary Fig. S1). Thus, the analyses appear to reveal meaningful functional contribution patterns of the VOIs despite confounding total lesion size.

The overall distribution of contribution values in the color-maps for the different methods (MSA, VLSM, VLSC) shows similar trends, with strong values for subcortical VOIs in the left hemisphere and left frontal cortex, suggesting strong contributions to the global behavioral score. On the other hand, there are clear differences between the maps, with, for example, high contributions of the right thalamus and right parietal cortex in the MSA, which do not appear as strongly in VLSM and VLSC. Moreover, the right putamen shows negative contributions in the MSA. Finally, we also computed the relative importance of VOIs for the accurate prediction of NIHSS from the multi-regional lesion patterns using the MAPP approach (results shown in Supplementary Material in Fig. S2).

3.5. Comparison of indicators of functional contributions

In order to obtain a more comprehensive overview of the functional contributions indicated by different lesion inference methods, Fig. 7 shows the normalized indicators of functional contributions (VLSM, VLSC, MAPP and MSA) for both hemispheres, sorted by increasing range of variation among them (VLSM-complete and MSA-complete indicators were computed as mean values over 77 (for left) and 72 (for right) leave-one-out predictions). The contribution values in each approach were normalized, by the sum of all regional contributions, to yield relative functional contributions.

The values of contributions obtained with MSA are the same as depicted in Fig. 4 and in the first row of Fig. 6. VLSM values were computed both for the complete-predicted dataset (VLSM-complete) with the leave-one-out technique as for MSA contributions, and for the binary-sample (VLSM-sample) dataset, as in Fig. 6. By contrast, VLSC, which uses graded lesion information, was calculated only for the original-sample (VLSC-sample) dataset, as in Fig. 6. MAPP contributions were calculated for the binary-sample (MAPP-sample) dataset and are also shown in Fig. S2 of the Supplementary Material. Note that in Fig. 7, all indicators are normalized, for comparison.

We also computed the Pearson correlation coefficients between the different indicators. For the left hemisphere, correlations that were significantly different from zero were between VLSM-complete and MSA-complete ($r = 0.97$, $p < 0.05$), between VLSM-sample and VLSC-sample ($r = 0.87$, $p < 0.05$), between VLSM-sample and VLSM-complete ($r = 0.83$, $p < 0.05$), between VLSM-sample and MSA-complete ($r = 0.84$, $p < 0.05$) and between VLSM-complete and VLSC-sample ($r = 0.74$, $p < 0.05$). The correlations between MSA-complete and VLSC-sample and all correlations between MAPP-sample and other indicators were not significantly different from zero ($p > 0.05$). For the right hemisphere, correlations that were significantly different from zero existed between VLSM-complete and MSA-complete ($r = 0.95$, $p < 0.05$), between VLSM-complete and VLSC-sample ($r = 0.73$, $p < 0.05$), between MSA-complete and VLSC-sample ($r = 0.70$, $p < 0.05$), between VLSM-complete and MAPP-sample ($r = 0.74$, $p < 0.05$) and between VLSC-sample and MAPP-sample ($r = 0.89$, $p < 0.05$). As shown in Fig. 7 and indicated by the correlation coefficients, the outcomes of VLSC-sample and VLSM-sample calculations were similar to each other, but mostly different from the MSA contributions. The results of the VLSM-complete compared to the VLSM-sample approach showed a highly significant relation with behavioral deficits for lesions of the bilateral caudate, parietal and frontal lobes, as well as lesions of the thalamus in the right hemisphere and insula in the left hemisphere. The results indicated that subcortical VOIs tended to have a larger range of variation across the five indicators (especially in the right hemisphere) and that the use of a complete set of lesion configurations for the VLSM approach produced similar contribution values as for the MSA (also confirmed by the high correlation coefficient), that however differed from the indicators computed on the original-sample dataset (VLSM-sample, VLSC-sample and MAPP-sample). This finding suggests that biases inherent to sample datasets may be ameliorated by taking into account all theoretically possible lesion configurations.

4. Discussion

In the present study, we systematically applied the MSA approach to an extensive stroke patient dataset and compared the method with other established lesion inference approaches. The results demonstrated characteristic functional contributions, particularly of subcortical structures, to basic behavioral functions as captured by the NIHSS, and show similarities as well as systematic differences between the MSA and established lesion inference approaches. This study extends a previous proof-of-concept study by Kaufman et al. (2009), in which the authors applied MSA to CT lesion data and line bisection test scores of 23 right-hemisphere stroke patients, by presently using a substantially larger patient sample (148 cases) in conjunction with a comprehensive clinical stroke score. Moreover, here we computed and discussed functional interactions derived from MSA, and performed a comparison of MSA outcomes with those from several other approaches.

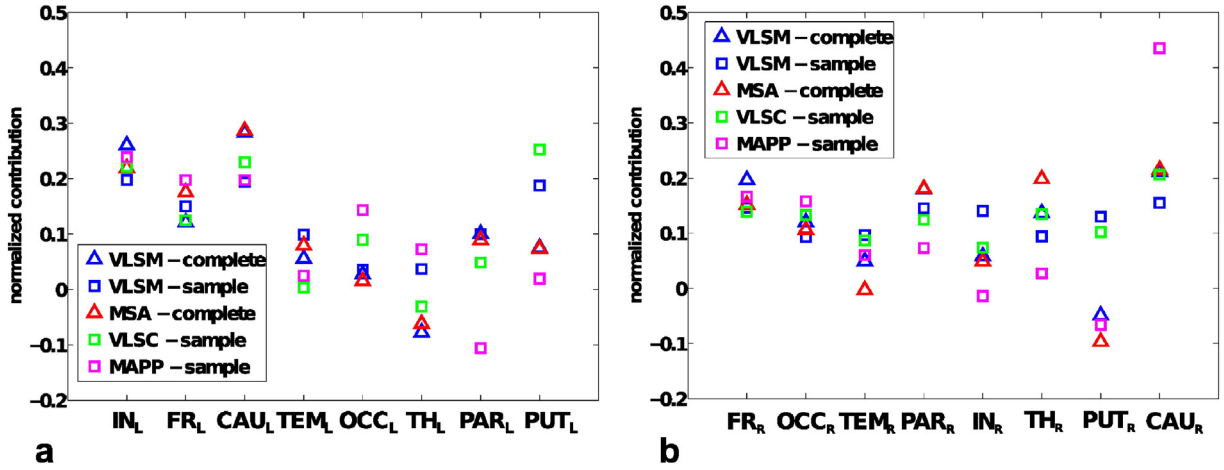

Fig. 7. Comparison of indicators of functional contributions. Normalized indicators of functional contributions, computed for sampled and complete-predicted datasets, sorted by increasing range of variation, for left and right hemispheres.

4.1. Main findings of the MSA approach

For all large-scale VOIs of the present study, contributions computed with MSA were significantly different from zero (with the exception of the right temporal lobe). In particular, subcortical regions, such as the bilateral caudate and insula, together with the parietal and frontal lobes, were inferred to make the strongest contributions to behavior as captured in the NIHSS. Interestingly, MSA also revealed negative contributions, specifically from the right putamen and left thalamus.

Motor symptoms (facial palsy together, weakness of arms and legs) result in high score values on the NIHSS and explain up to 18 of 42 possible score points. Thus, as described previously, we would expect high contribution values in VOIs that comprise the pyramidal tract as well as cortical brain regions involved in motor function, for example, primary and secondary motor areas (Menezes et al., 2007; Zhu et al., 2010; Cho et al., 2007). This aspect may explain the strong contribution of the bilateral frontal VOI which comprises cortical motor brain areas in our analysis. The strong contribution of the left insula reflects the association of insular infarction with stroke severity that has been reported in Fink et al. (2005). Insular infarction is frequently observed in the context of large non-lacunar stroke and, thus, often comes along with larger stroke volumes that cause greater neurological deficits, due to proximal MCA occlusion.

Regarding the strong contribution of the caudate nucleus observed in the present analysis, there are only few studies investigating isolated caudate infarctions (Kumral et al., 1999). However, we suggest that the effects observed with our results might stem from involvement of the internal capsule, more specifically the "genu" that contains corticobulbar tracts connecting primary motor areas to the nuclei of cranial nerves, which are involved in motor function and language performance, among other functions. Damage to both the genu of the internal capsule and parts of the caudate would specifically occur in proximal MCA occlusions, where the lateral lenticulostriate artery supporting both structures is blocked. Once again, we would, therefore, at least in part observe an effect of proximal MCA occlusions that mostly involve the basal ganglia including the caudate nucleus (Cheng et al., 2011).

We noted stronger contribution values for left hemispheric VOIs. These values could be related to the fact that larger infarctions of the left (dominant) hemisphere and MCA territory cause disturbances of speech, whereas right-sided cortical infarctions are more often associated with spatial neglect. This imbalance might have been promoted by the design of the NIHSS that awards 7 out of 42 points on abilities that require verbal skills (Woo et al., 1999), so that aphasia, which most frequently occurs in left hemispheric stroke, leads to comparatively high NIHSS values, while neglect, most frequently resulting from right hemispheric stroke lesions, only scores a maximum of 2 points on the NIHSS.

Moreover, we observed the highest contribution values for subcortical structures, which may be partly explained by the definition of VOIs used in the current analysis. Particularly, the basal ganglia VOI (putamen, caudate) as defined in the MNI atlas comprise adjacent white matter brain areas such as the internal capsule, and it is well known that stroke lesions affecting the internal capsule often result in severe motor symptoms (Fries et al., 1993; Lee et al., 2005). Moreover, strong contributions of subcortical regions may also relate to the distribution of acute MCA strokes, which mainly involve subcortical structures while the frequency of involvement decreases towards the cortical brain areas as shown in the regional distribution of lesions in our sample as well as in previous reports (Cheng et al., 2011). Finally, this finding may reflect aspects of brain architecture that concentrate strategic fiber tracts in small vicinities in subcortical brain regions, which may result in severe symptoms even in case of small lesion volumes. We also identified specific differences as to the contribution of homologous brain regions in the left and right hemisphere. This observation may partly result from the asymmetric representation of left and right hemispheric brain functions in the NIHSS, but might also point towards specific lateralized features of brain organization.

The exact MSA approach requires full information of all 2^N binary brain state configurations, where N is the number of regions of interest, with corresponding performance scores. Thus, ideally, one would have available information from 2^N patients, whose lesion patterns are all different from each other. These numbers quickly increase with the number of elements of interest, restricting the maximum number of VOIs used in the analysis. In the present study, we chose a set of eight large-scale, well-defined VOIs for each hemisphere that are readily available in the MNI atlas and that provide a complete, non-overlapping parcellation of the brain. Some of these VOIs include gray as well as white matter. In part, these VOIs are quite large and encompass numerous functionally relevant but disjoint brain areas (e.g., frontal cortex). As a result, the functional contributions that we identified represent the sum of functional contributions of gray matter regions comprised by the VOI as well as white matter tracts running through them.

We also identified VOIs with negative contributions to the NIHSS sum score, particularly the right putamen and left thalamus, a finding that is not readily explained in the context of acute stroke. As the thalamus is mainly supplied by the posterior cerebral artery/basilary artery (Schmahmann, 2003), combined damage to the thalamus and internal capsule is less common. This fact might in part explain the negative contribution of the thalamus at least on the left side. A more speculative interpretation would be that involvement of multiple subcortical components (that is, infarction of the caudate nucleus as well as the thalamus) would activate networks of subcortical-cortical regions via release from inhibition, leading to lower clinical impairment. Similar effects can be seen in virtual lesion experiments involving TMS (Hilgetag et al., 2001). However, given the limitations of the VOIs used in our study, one needs to be cautious in interpreting these preliminary results. Further studies are necessary that apply the MSA approach to refined VOIs, which are more specifically tailored to the studied behavioral performance and also take into account gray as well as white matter parcellations.

A refinement of the VOIs can start from inspecting the functional interactions. Regions that show redundant interactions are partly functionally overlapping and may be merged or redrawn into more appropriate functional parcels. On the other hand, regions that show synergistic interactions should be kept separate. Interestingly, there were differences between the significant interactions among VOIs in the left and right hemispheres, which may be due to the lateralization of functions assessed by the NIHSS. In the present analysis, the strongest redundant interactions were between the caudate and the frontal and parietal lobes in the left hemisphere, and between the frontal lobe and parietal lobe, insula and thalamus in the right hemisphere. These regions have largely independent lesion patterns, as shown by an absence of significant correlations between the relative lesion patterns (Fig. S3 in Supplementary Material). This observation suggests that the functional overlap indicated by the redundant functional interactions is not just due to lesion pattern covariance, perhaps induced by placement in the same infarct territory, but reflects genuine functional overlap.

4.2. Advantages and drawbacks of different lesion inference methods

One aim of this study was to compare inferences made by MSA to other lesion inference methods. It should be emphasized that a direct, quantitative comparison of the accuracy and reliability of the different methods in inferring functional contributions is impossible without ground truth knowledge about the actual contributions, which are unknown for this clinical sample. Therefore, an objective evaluation of the relative performance of different lesion analysis approaches needs be performed in a separate project, in which the ground truth contributions can be defined a priori (Mah et al., 2014). However, while the current study cannot directly evaluate the relative accuracy of the approaches, it shows the variety in functional contributions that are computed by different inference techniques. While the overall pattern of

contributions was comparable among the different approaches, there were also remarkable differences. In order to understand these findings, one needs to take into account methodological differences between the approaches as well as general limitations of lesion inferences.

The use of clinical data typically carries a *sample bias*. In fact, while MSA as used in this work is based on the complete-predicted dataset containing all possible lesion states, VLSC, VLSM or MAPP do not require such a complete dataset, but use the original-sample and binary-sample datasets. As discussed, we applied VLSM also to the complete-predicted dataset and compared the results with the MSA contributions. For VLSC it was not possible to use the complete-predicted dataset, because the correlations are necessarily computed on the graded data. Similar to the MSA, the approach of VLSC confirmed the pivotal role of subcortical regions as well as the general predominance of left-hemispheric regions in the functions assessed by NIHSS; but, differently from MSA, bilateral thalamus and occipital lobe were not significantly correlated with the global NIHSS. Also, MAPP showed similar results compared to MSA, especially in right hemisphere, but also differences, such as the role of parietal lobe in left hemisphere. The results of VLSC, MAPP and VLSM applied to sample datasets showed similar results to each other, as well as a general difference in comparison with MSA contributions. The fact that VLSM, VLSC and MAPP do not use the complete space of configurations means they are subject to sample biases, potentially resulting in false positives and negatives. However, when VLSM was applied to the complete-predicted dataset, it showed similar results as the MSA, with significant functional contributions for the left subcortical regions and the left frontal cortex as well as the right caudate, frontal, parietal cortex and thalamus. These results demonstrate that the use of a complete set of lesion cases may lead to results that are less affected by a potential sample bias.

A further *estimation bias* is intrinsic to methods that compute bivariate contributions or correlations. This bias could be corrected, for example, by using *partial correlations* (Baba et al., 2004) among the VOIs and additional factors, rather than bivariate correlations. The partial correlation results would quantify the degree of association between lesion size in a VOI and the behavioral scores, while accounting for the influence of further variables (e.g., variation of lesion size in other regions) on this relationship. Such corrections would require a more elaborate statistical analysis as part of the VLSM and VLSC approaches, which usually is not performed in these analyses, but is already intrinsic to the multivariate MSA and MAPP approaches.

Generally, MSA possesses some appealing features compared to alternative inference methods. MSA uses a principled mathematical approach that makes the assignment of contributions to regions transparent, compared to the assignment of values in machine learning approaches. Moreover, MSA takes into account all regions and their interactions, unlike bivariate approaches such as VLSM and VLSC, and provides an exact and unique assignment of contribution values if all lesion configurations are known.

However, MSA also has drawbacks compared to alternative methods of lesion inference. The main disadvantage is the preparation of the complete lesion dataset that is typically required by the algorithm, potentially resulting in a *prediction bias* from the machine-learning estimation of a complete dataset of 2^N lesion states and corresponding scores. VLSM and VLSC, instead, do not require the prediction of performance scores for all possible configurations, and therefore can also be applied to a larger number of VOIs, or to lesion data sampled at the voxel level. However, variants of the MSA approach exist that are based on incomplete samples of the space of all lesion configurations (Keinan et al., 2006). The applicability of this modified approach to problems involving up to 100 nodes has been demonstrated (Keinan et al., 2006); however, it still remains a challenge to scale the approach to the number of elements involved in voxel-based approaches.

Finally, a problem common to all methods is due to the fact that clinical data used in lesion inference analyses may suffer from a *selection bias*. This bias arises when only patients with functional deficits are included in the analysis, while ignoring subjects with lesions but without deficits. However, the latter cases are essential for excluding the redundant contributions of some of the lesioned structures that are damaged as a consequence of an infarct, but may not actually be causally contributing to behavioral deficits. In lesion studies of specific deficits, such as aphasia or spatial neglect, this bias can be controlled by including brain-damaged patients without the specific syndrome under consideration; for instance, stroke patients that are aphasic but have intact spatial attention could be included in a neglect study. However, such a balancing of the patient sample is difficult when using broad, multifunctional clinical scores such as the NIHSS. Therefore, all functional inferences in the present study, including the ones made by MSA, suffer from a bias towards false positives.

4.3. Further limitations

It should be emphasized that only diffusion-weighted MRI datasets were used in this study for lesion delineation and subsequent analysis. In the setting of an acute stroke, brain cells located within a lesion visible in diffusion-weighted MRI are typically assumed to represent the infarct core, which is not salvageable. Complementary to this approach, perfusion-weighted MRI is used to obtain knowledge about the hypoperfused tissue. The volumetric mismatch between these two lesions can be used as a surrogate for the ischemic penumbra. Brain cells in this region are assumed to be salvageable, if reperfusion is achieved. However, it is still a matter of debate to what extent brain cells in this area are still functional. For example, Marshall et al. (2001) found that the residual function of brain cells varied with the absolute cerebral blood flow pattern. It could be hypothesized that the diffusion lesions used in the present study underestimate the extent of inactivated brain cells and, thus, do not completely explain the functional deficit. Although it would be interesting to explore this issue in more detail, it needs to be highlighted that, in contrast to the characterization of lesions in diffusion-weighted MRI datasets, which is straightforward, the optimal definition of the hypoperfused tissue is still a matter of debate. Particularly, several sets of different perfusion parameters and thresholds have been proposed for the definition of the hypoperfused tissue (Forkert et al., 2013). Thus, the choice of the perfusion parameter (e.g., cerebral blood flow or time-to-peak) and threshold used for identification of the hypoperfusion may considerably influence the outcome of all lesion mapping techniques, while it remains unclear if all brain cells within the hypoperfused brain tissue are indeed inactive brain cells. Therefore, a perfusion lesion may overestimate the functionally relevant lesion. In contrast to this, one can be confident that cells within the diffusion lesion are inactive. Ultimately, the use of very many different configurations of focal diffusion lesions as in the present study might approximate the same configuration space as that resulting from large perfusion lesions, due to the use of the lesion overlap median value for binarization of lesioned brain regions, as perfusion lesions are typically located around the diffusion lesion, but are larger. In conclusion, although the issue of characterization of stroke lesions by diffusion versus perfusion imaging needs to be analyzed in more detail in further studies, we are confident that the present analysis already provides worthwhile knowledge about the functional importance of different brain regions.

4.4. General conclusions

The MSA approach allows the objective, game-theory based computation of regional causal contributions to brain function. In the present study, we demonstrated that MSA can be applied to clinical datasets for stroke lesions, to reveal characteristic contribution patterns of large-scale VOIs to a broad range of behavioral and cognitive functions as reflected in the NIHSS. The results deepen the understanding of the functional impact of regionally specific brain lesions to the NIHSS and, thus, contribute to the use of this scale in clinical practice and research.

We showed that alternative measures of lesion inference produce broadly similar functional contributions, but differ in the detailed ranking of contributions. The comparison of indicators of functional contributions derived from the original, restricted as well as the predicted complete sets of lesion configurations also revealed differences. In comparison to other techniques, the MSA approach, as employed here, has the practical limitation that it needs to be computed from the complete space of all combinations of intact or lesioned regions. This requirement can be satisfied through the combination of the approach with a predictive algorithm for deriving the scores corresponding to all possible lesion configurations from the known configurations, at the expense of a prediction bias. We also identified points for further research, such as the selection of VOIs that requires further refining.

In summary, we suggest that MSA can be used as a valid alternative to established lesion inference approaches, due to its robust intrinsic mathematical basis and its potential to overcome biases of bivariate associations inherent in alternative approaches. The present preliminary results indicate the potential of the MSA approach for improving the understanding of the localization of essential brain functions as well as providing useful guidance for stroke patient treatment and rehabilitation.

Statement of compliance

PRE-FLAIR — the study was approved by the local ethics committees at all centers. Either written or verbal informed consent was obtained for all patients, as required by local legislation.

Conflicts of interest

Christian Gerloff has received fees as a consultant or lecture fees from Bayer Vital, Boehringer Ingelheim, EBS technologies, Glaxo Smith Kline, Lundbeck, Pfizer, Sanofi Aventis, Silk Road Medical, and UCB. Götz Thomalla has received fees as a consultant or lecture fees from Covidien and Boehringer Ingelheim.

Acknowledgments

Research was supported by the ERA-NET NEURON project “BEYONDVIS” (BMBF 01EW1002) and the SFB 936 “Multi-site Communication in the Brain” (Projects A1, C2). We thank Jan Gläscher for helpful comments on the manuscript.

Appendix A. Supplementary data

Supplementary data to this article can be found online at http://dx.doi.org/10.1016/j.nicl.2015.07.009.

References

Baba, K., Shibata, R., Sibuya, M., 2004. Partial correlation and conditional correlation as measures of conditional independence. Aust. N. Z. J. Stat. 46 (4), 657–664. http://dx.doi.org/10.1111/j.1467-842X.2004.00360.x.

Bates, E., Wilson, S.M., Saygin, A.P., Dick, F., Sereno, M.I., Knight, R.T., Dronkers, N.F., 2003. Voxel-based lesion-symptom mapping. Nat. Neurosci. 6 (5), 448–450. http://dx.doi.org/10.1038/nn105012704393.

Besl, P.J., McKay, H.D., 1992. A method for registration of 3-D shapes. I.E.E.E. Transactions Pattern Anal. Mach. Intell. 14 (2), 239–256. http://dx.doi.org/10.1109/34.121791.

Brott, T., Adams, H.P., Olinger, C.P., Marler, J.R., Barsan, W.G., Biller, J., Spilker, J., Holleran, R., Eberle, R., Hertzberg, V., 1989. Measurements of acute cerebral infarction: a clinical examination scale. Stroke 20 (7), 864–870. http://dx.doi.org/10.1161/01.STR.20.7.8642749846.

Chang, C.-C., Lin, C.-J., 2011. LIBSVM: a Library for Support Vector Machines. A.C.M. Transactions Intell. Syst. Technol. 2 (3), 1–27. http://dx.doi.org/10.1145/1961189.1961199.

Cheng, B., Brinkmann, M., Forkert, N.D., Treszl, A., Ebinger, M., Köhrmann, M., Wu, O., Kang, D.-W., Liebeskind, D.S., Tourdias, T., Singer, O.C., Christensen, S., Luby, M., Warach, S., Fiehler, J., Fiebach, J.B., Gerloff, C., Thomalla, G., STIR and VISTA Imaging Investigators, 2013. Quantitative measurements of relative fluid-attenuated inversion recovery (FLAIR) signal intensities in acute stroke for the prediction of time from symptom onset. J. cereb. blood flow metab. 33 (1), 76–84. http://dx.doi.org/10.1038/jcbfm.2012.12923047272.

Cheng, B., Golsari, A., Fiehler, J., Rosenkranz, M., Gerloff, C., Thomalla, G., 2011. Dynamics of regional distribution of ischemic lesions in middle cerebral artery trunk occlusion relates to collateral circulation. J. cereb. blood flow metab. 31 (1), 36–40. http://dx.doi.org/10.1038/jcbfm.2010.18520940728.

Cho, S.-H., Kim, D.G., Kim, D.-S., Kim, Y.-H., Lee, C.-H., Jang, S.H., 2007. Motor outcome according to the integrity of the corticospinal tract determined by diffusion tensor tractography in the early stage of corona radiata infarct. Neurosci. Lett. 426 (2), 123–127. http://dx.doi.org/10.1016/j.neulet.2007.08.04917897782.

Collins, D.L., Holmes, C.J., Peters, T.M., Evans, A.C., 1995. Automatic 3-D model-based neuroanatomical segmentation. Hum. Brain Mapp. 3 (3), 190–208. http://dx.doi.org/10.1002/hbm.460030304.

De Freitas, G.R., De, H., Christoph, D., Bogousslavsky, J., 2009. Topographic classification of ischemic stroke. Handbook of clinical. Neurology 93, 425–452.

Fink, J.N., Selim, M.H., Kumar, S., Voetsch, B., Fong, W.C., Caplan, L.R., 2005. Insular cortex infarction in acute middle cerebral artery territory stroke: predictor of stroke severity and vascular lesion. Arch. Neurol. 62 (7), 1081–1085. http://dx.doi.org/10.1001/archneur.62.7.108116009763.

Forkert, N.D., Kaesemann, P., Treszl, A., Siemonsen, S., Cheng, B., Handels, H., Fiehler, J., Thomalla, G., 2013. Comparison of 10 TTP and Tmax estimation techniques for MR perfusion-diffusion mismatch quantification in acute stroke. A.J.N.R. Am. J. Neuroradiol. 34 (9), 1697–1703. http://dx.doi.org/10.3174/ajnr.A3460235338410.

Forkert, N.D., Säring, D., Fiehler, J., Illies, T., Möller, D., Handels, H., 2009. Automatic brain segmentation in time-of-flight MRA images. Methods Inform. Med. 48 (5), 399–407. http://dx.doi.org/10.3414/ME923719696951.

Fries, W., Danek, A., Scheidtmann, K., Hamburger, C., 1993. Motor recovery following capsular stroke. Role of descending pathways from multiple motor areas. Brain 116 (2), 369–3828461971.

Hilgetag, C.C., Théoret, H., Pascual-Leone, A., 2001. Enhanced visual spatial attention ipsilateral to rTMS-induced ‘virtual lesions’ of human parietal cortex. Nat. Neurosci. 4 (9), 953–957. http://dx.doi.org/10.1038/nn0901-95311528429.

Karnath, H.-O., Ferber, S., Himmelbach, M., 2001. Spatial awareness is a function of the temporal not the posterior parietal lobe. Nature 411 (6840), 950–953. http://dx.doi.org/10.1038/3508207511418859.

Kaufman, A., Keinan, A., Meilijson, I., Kupiec, M., Ruppin, E., 2005. Quantitative analysis of genetic and neuronal multi-perturbation experiments. PLOS Comput. Biol. 1 (6), e64. http://dx.doi.org/10.1371/journal.pcbi.001006416322764.

Kaufman, A., Serfaty, C., Deouell, L.Y., Ruppin, E., Soroker, N., 2009. Multiperturbation analysis of distributed neural networks: the case of spatial neglect. Hum. Brain Mapp. 30 (11), 3687–3695. http://dx.doi.org/10.1002/hbm.2079719449335.

Keinan, A., Kaufman, A., Sachs, N., Hilgetag, C.C., Ruppin, E., 2004b. Fair localization of function via multi-lesion analysis. Neuroinformatics 2 (2), 163–168. http://dx.doi.org/10.1385/NI:2:2:16315319513.

Keinan, A., Sandbank, B., Hilgetag, C.C., Meilijson, I., Ruppin, E., 2004a. Fair attribution of functional contribution in artificial and biological networks. Neural Comput. 16 (9), 1887–1915. http://dx.doi.org/10.1162/089976604133638715265327.

Keinan, A., Sandbank, B., Hilgetag, C.C., Meilijson, I., Ruppin, E., 2006. Axiomatic scalable neurocontroller analysis via the Shapley value. Artif. Life 12 (3), 333–352. http://dx.doi.org/10.1162/artl.2006.12.3.33316859444.

Kümmerer, D., Hartwigsen, G., Kellmeyer, P., Glauche, V., Mader, I., Klöppel, S., Suchan, J., Karnath, H.-O., Weiller, C., Saur, D., 2013. Damage to ventral and dorsal language pathways in acute aphasia. Brain J. neurol. 136 (2), 619–629. http://dx.doi.org/10.1093/brain/aws35423378217.

Kumral, E., Evyapan, D., Balkir, K., 1999. Acute caudate vascular lesions. Stroke 30 (1), 100–108. http://dx.doi.org/10.1161/01.STR.30.1.1009880396.

Lee, J.S., Han, M.K., Kim, S.H., Kwon, O.K., Kim, J.H., 2005. Fiber tracking by diffusion tensor imaging in corticospinal tract stroke: topographical correlation with clinical symptoms. Neuroimage 26 (3), 771–776. http://dx.doi.org/10.1016/j.neuroimage.2005.02.03615955486.

Lorensen, W.E., Cline, H.E., 1987. Marching cubes: a high resolution 3D surface construction algorithm. Computer 21 (4), 163–169. http://dx.doi.org/10.1145/37402.37422.

Mah, Y.H., Husain, M., Rees, G., Nachev, P., 2014. Human brain lesion-deficit inference remapped. Brain 137 (9), 2522–2531. http://dx.doi.org/10.1093/brain/awu16424974384.

Marshall, R.S., Lazar, R.M., Pile-Spellman, J., Young, W.L., Duong, D.H., Joshi, S., Ostapkovich, N., 2001. Recovery of brain function during induced cerebral hypoperfusion. Brain J. neurol. 124 (6), 1208–1217. http://dx.doi.org/10.1093/brain/124.6.120811353736.

Menezes, N.M., Ay, H., Wang Zhu, M., Lopez, C.J., Singhal, A.B., Karonen, J.O., Aronen, H.J., Liu, Y., Nuutinen, J., Koroshetz, W.J., Sorensen, A.G., 2007. The real estate factor: quantifying the impact of infarct location on stroke severity. Stroke 38 (1), 194–197. http://dx.doi.org/10.1161/01.STR.0000251792.76080.4517122428.

Rorden, C., Brett, M., 2000. Stereotaxic display of brain lesions. Behav. Neurol. 12 (4), 191–200. http://dx.doi.org/10.1155/2000/421719115684 31.

Rorden, C., Fridriksson, J., Karnath, H.-O., 2009. An evaluation of traditional and novel tools for lesion behavior mapping. NeuroImage 44 (4), 1355–1362. http://dx.doi.org/10.1016/j.neuroimage.2008.09.03118950719.

Rorden, C., Karnath, H.-O., 2004. Using human brain lesions to infer function: a relic from a past era in the fMRI age? Nat. Rev. Neurosci. 5 (10), 813–819. http://dx.doi.org/10.1038/nrn152115378041.

Saver, J.L., Johnston, K.C., Homer, D., Wityk, R., Koroshetz, W., Truskowski, L.L., Haley, E.C., 1999. Infarct volume as a surrogate or auxiliary outcome measure in ischemic stroke clinical trials. The RANTTAS Investigators. Stroke 30 (2), 293–298. http://dx.doi.org/10.1161/01.STR.30.2.2939933262.

Schmahmann, J.D., 2003. Vascular syndromes of the thalamus. Stroke 34 (9), 2264–2278. http://dx.doi.org/10.1161/01.STR.0000087786.38997.9E12933968.
Shapley, L.S., 1953. Stochastic games. Proc. Natl. Acad. Sci. U. S. A. 39 (10), 1095–1100. http://dx.doi.org/10.1073/pnas.39.10.109516589380.
Smith, D.V., Clithero, J.A., Rorden, C., Karnath, H.-O., 2013. Decoding the anatomical network of spatial attention. Proc. Natl. Acad. Sci. U. S. A. 110 (4), 1518–1523. http://dx.doi.org/10.1073/pnas.121012611023300283.
Thomalla, G., Cheng, B., Ebinger, M., Hao, Q., Tourdias, T., Wu, O., Kim, J.S., Breuer, L., Singer, O.C., Warach, S., Christensen, S., Treszl, A., Forkert, N.D., Galinovic, I., Rosenkranz, M., Engelhorn, T., Köhrmann, M., Endres, M., Kang, D.W., Dousset, V., Sorensen, A.G., Liebeskind, D.S., Fiebach, J.B., Fiehler, J., Gerloff, C., 2011. DWI-FLAIR mismatch for the identification of patients with acute ischaemic stroke within 4·5 h of symptom onset (PRE-FLAIR): a multicentre observational study. Lancet Neurol. 10 (11), 978–986. http://dx.doi.org/10.1016/S1474-4422(11)70192-221978972.
Woo, D., Broderick, J.P., Kothari, R.U., Lu, M., Brott, T., Lyden, P.D., Marler, J.R., Grotta, J.C., 1999. Does the National Institutes of Health Stroke Scale favor left hemisphere strokes? NINDS t-PA Stroke Study Group. Stroke 30 (11), 2355–2359. http://dx.doi.org/10.1161/01.STR.30.11.235510548670.
Zhu, L.L., Lindenberg, R., Alexander, M.P., Schlaug, G., 2010. Lesion load of the corticospinal tract predicts motor impairment in chronic stroke. Stroke 41 (5), 910–915. http://dx.doi.org/10.1161/STROKEAHA.109.57702320378864.